International Journal of Solids and Structures 50 (2013) 1364–1372

Contents lists available at SciVerse ScienceDirect

International Journal of Solids and Structures

journal homepage: www.elsevier.com/locate/ijsolstr

Cavitation instabilities in bulk metallic glasses

X. Huang, Z. Ling, L.H. Dai *

State Key Laboratory of Nonlinear Mechanics, Institute of Mechanics, Chinese Academy of Sciences, Beijing 100190, China

ARTICLE INFO

Article history:
Received 17 October 2012
Received in revised form 13 December 2012
Available online 24 January 2013

Keywords:
Void growth
Metallic glasses
Dynamic fracture
Free volume

ABSTRACT

To reveal the mechanism of a void-dominated fracture process in bulk metallic glasses, a theoretical description of void growth undergoing remote hydrostatic tension is presented. Special attention is focused on cavitation instabilities and dynamics of a dynamic void growth process. The critical stress for cavitation instabilities is derived theoretically, which is validated by numerical simulations with a finite difference method. To characterize the dynamic void growth process, a dimensionless number is proposed, which embodies the competition of inertial effects, loading rate effects and viscous effects. It is found that inertial effects can induce vibration of the void growth rate at the rise stage of loading history and impede the growth at the steady stage. In addition, to study the void growth at the early stage of a void-dominated fracture process, quasistatic cases without inertial effects are examined. It is shown that the void growth rate strongly depends on the evolution of free volume concentration.

1. Introduction

In polycrystalline alloys, ductile fracture is attributed to nucleation, growth and coalescence of micro-voids. To understand a void-dominated fracture process, the void growth has been widely investigated over the last few decades. Hill (1950) performed a classical analysis of void growth under static loading, and obtained an explicit expression between the applied internal pressure and void radius. Carroll and Holt (1972) examined the collapse of a void in a sphere of ideally plastic material under external pressure, and indicated that the influence of elastic compressibility on void collapse is very small. Based on the Carroll and Holt approach, Johnson (1981) studied void growth in a rate-dependent material under dynamic tensile loading to describe the spallation behavior of solids. As research went further, more complicated cases of void growth were considered and much attention was paid on a bifurcation phenomenon – cavitation instabilities. Ball (1982) recognized the existence of cavitation instabilities. It was interpreted as a bifurcation from a defect-free solid to a solid containing a void. Horgan and Abeyaratne (1986) presented an alternative physical interpretation for the phenomenon that was regarded as the unbounded growth of a pre-existing void. Huang et al. (1991) investigated cavitation instabilities in elastic–plastic materials under hydrostatic tension and axisymmetric loading, and found that the criterion for cavitation depends on a critical value of the mean stress. Their investigation was subsequently extended to more complicated cases where the initial void shape and the interaction between voids were considered (Tvergaard, 2012; Tvergaard et al., 1992; Tvergaard and Hutchinson, 1993; Tvergaard and Vadillo, 2007). To understand the effects of inertia, strain hardening and rate dependence, Ortiz and Molinari (1992) studied void growth in a power-law hardening material and indicated that inertia effects tend to dominate the long-term response of void growth. Molinari and Mercier (2001) further proposed a multiscale model to describe the behavior of porous materials. Taking the effects of growing voids into account, the influence of micro inertial effects on the microscopic response was addressed. Recently, Wu et al. (2003a,b,c) made a comprehensive work on the dynamic void growth with particular attention on thermal, inertial and rate-dependent effects, and indicated that thermal effects are strongly affected by initial void size, while inertial effects depend on the void size and loading rate.

In contrast, research on the void-dominated fracture process in bulk metallic glasses (BMGs) is still limited. For the unique disordered atomic structures (Chen, 2008; Egami, 2011; Falk and Langer, 2011; Greer, 1995; Greer and Ma, 2007; Greer and De Hosson, 2011; Johnson, 1999; Spaepen, 2006; Wang, 2012), plastic deformation is prone to be localized into thin shear bands in BMGs (Argon, 1979; Dai and Bai, 2008; Dai et al., 2005; Gao et al., 2011, 2007; Han et al., 2009; Huang et al., 2002; Jiang and Dai, 2009, 2011; Joshi and Ramesh, 2008; Liu et al., 2005; Ruan et al., 2011; Spaepen, 1977). Hence the fracture process (Chen et al., 2011; Martin et al., 2008, 2006; Schuh et al., 2007; Trexler and Thadhani, 2010) of BMGs is usually undergoing highly localized deformation via formation and rapid propagation of shear bands. In fact, BMGs can also fail by nucleation, growth and coalescence of microvoids. Bouchaud et al. (2008) conducted a quasistatic tension experiment

* Corresponding author. Tel.: +86 10 82543958; fax: +86 10 82543977.
E-mail address: lhdai@lnm.imech.ac.cn (L.H. Dai).

0020-7683/$ - see front matter © 2013 Elsevier Ltd. All rights reserved.
http://dx.doi.org/10.1016/j.ijsolstr.2013.01.011

on a Zr-based metallic glass (Vit. 1) and typical dimple patterns with diameter from 10^2 nm to micrometer scale were observed on the fracture surfaces of tested samples. The mismatch between two opposite fracture surfaces showed that the final fracture is controlled by growth and coalescence of damage cavities. Jiang et al. (2008, 2010a, 2010b) examined fracture patterns of Vit. 1 in compression, tensile and plate impact experiments. Fine 100 nm size dimples, nanoscale periodic corrugations and honeycomb structures were observed on dynamic mode I fracture surfaces. Based on these fracture patterns, a new atomic motion unit called as tension transformation zone (TTZ) was proposed to understand the nucleation of nanoscale voids ahead of a crack tip. Similar phenomenon has been observed in spallation experiments (Escobedo and Gupta, 2010; Huang et al., 2011; Turneaure et al., 2007; Zhuang et al., 2002). Huang et al. (2011) studied the spallation behavior of a Zr-based metallic glass (Vit. 1) via plate-impact experiments. Equiaxed cellular patterns with an average diameter of 2 μm were found on the spall surface of recovered samples, implying that the spallation is induced by nucleation, growth and coalescence of microvoids. Moreover, this microvoid dominated fracture process has been addressed in atomic scale by molecular dynamics (MD) simulations (An et al., 2011; Arman et al., 2010; Murali et al., 2011). Arman et al. (2010) investigated the dynamic response of a CuZr metallic glass with MD simulations and found that spallation process of this material is accompanied by nucleation and growth of microvoids. To reveal the intrinsic mechanism that governs the fracture process in brittle and ductile metallic glasses, Murali et al. (2011) performed MD simulations on two typical metallic glasses, FeP and CuZr. For the high degree of atomic scale spatial fluctuations, even the brittle FeP glass can fracture through nucleation and coalescence of multiple voids.

To understand the void-dominated fracture mechanism, research on void growth in BMGs is important. Steif (1983) studied an elliptical hole problem under plane strain tension to get insight into ductile vs brittle behavior in BMGs. He found that the hydrostatic tension can decrease viscosity and alleviates the severe stress conditions prevailing near potential cleavage flaws. Wright et al. (2003) proposed a model of void formation in shear bands of BMGs, and indicated that excess free energy exists in shear bands and void nucleation is duo to the coalescence of free volume. Their work addressed that the free volume concentration has a remarkable influence on the void growth rate. Bouchbinder et al. (2008) investigated cavitation instabilities in BMGs. Based on the athermal shear transformation zone theory (Bouchbinder et al., 2007a,b), they predicted the existence of fast cavitation modes accompanied by extensive plastic deformation. These pioneer works provide the important information for understanding the void growth in BMGs. However, there are still some basic questions that have not been answered. As BMGs are pressure sensitive solids with the unique plastic deformation mechanism, what is the criterion for cavitation instabilities? What are the dominant factors that determine the void growth rate? And how does the free volume dynamics affect a void growth process?

In this paper, we investigate the growth of a single void in BMGs under remote tensile loading to understand the void-dominated fracture process. An elastic-viscoplastic constitutive law with an internal parameter, free volume concentration, is adopted. The critical stress for cavitation instabilities is determined theoretically, and is validated numerically with a finite difference method. In order to reveal the dominant factors that influence the growth rate, we investigate the dynamic void growth under transient loading. A dimensionless inertial number is presented to characterize the dynamic void growth process, and numerical simulations were carried out to quantify the effects of dominant factors. In addition, to study the void growth at the early stage of a void-dominated fracture process, quasistatic cases without inertial effects are examined, and the influence of free volume dynamics on growth rate is discussed.

2. Basic model

Let us consider a spherical void of radius a in an infinite metallic glass under the remote hydrostatic tensile pressure p^{app}, as shown in Fig. 1. The void grows as the hydrostatic tensile pressure is applied. It is assumed that the void remains spherical throughout the growth process. Once the void surface yields, the elastic-viscoplastic boundary is considered as a spherical surface propagating outwards. Then, according to continuum mechanics, the equation of motion is written as:

$$\frac{d\sigma_r}{dr}+\frac{2}{r}(\sigma_r-\sigma_\theta)=\rho\ddot{r} \tag{1}$$

Compared with conventional polycrystalline alloys, where the carrier of the plastic deformation is a dislocation-like defect, the fundamental carriers of plastic deformation of BMGs are shear transformation zones (Argon, 1979; Falk and Langer, 1998; Pan et al., 2008) or flow defects (Spaepen, 1977, 2006). Thus, to describe the matrix material surrounding the void, an elastic-viscoplastic constitutive law is adopted as:

$$\varepsilon_{ij}=\frac{s_{ij}}{2\mu}\ \text{if}\ \tau+Qp\leqslant\hat{\tau}-(C_1T/T_g)^{1/2} \tag{2}$$

$$\dot{\varepsilon}_{ij}=\frac{\dot{s}_{ij}}{2\mu}+\frac{s_{ij}}{2\eta}\ \text{if}\ \tau+Qp\geqslant\hat{\tau}-(C_1T/T_g)^{1/2} \tag{3}$$

where ε_{ij} is the strain tensor, s_{ij} is the stress deviator, μ is the shear modulus, and η is the viscosity. To characterize the pressure sensitivity in plastic flow, the yield criterion of BMGs suggested by Sun et al. (2010) is used. In this criterion, $\tau=(\sigma_\theta-\sigma_r)/2$ is the maximum shear stress (σ_θ and σ_r are the principle stresses), $p=(\sigma_r+2\sigma_\theta)/3$ is the hydrostatic pressure, Q is the pressure sensitivity coefficient and the term $\hat{\tau}-(C_1T/T_g)^{1/2}$ represents the yield strength ($\hat{\tau}$ is the barrier shear resistance of a STZ, C_1 is a coefficient that reflects the temperature dependence of strength, T is the temperature, and T_g is the glass transition temperature).

To apply the conventional flow equation to multiaxial stress states, Steif (1983) modified the flow equation presented by Spaepen (1977), and defined the stress dependent viscosity as:

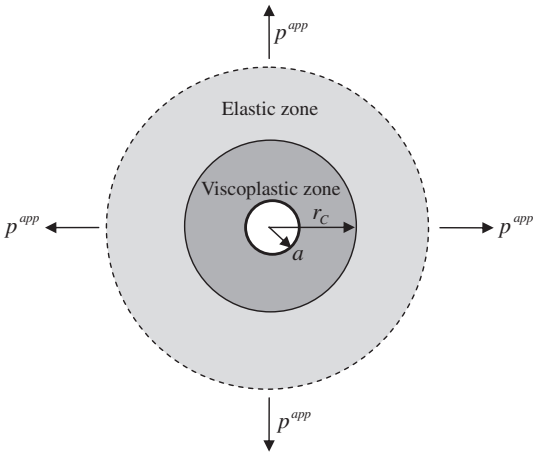

Fig. 1. Schematic diagram of a single void in an infinite body under remote hydrostatic tensile pressure. a is the void radius, p^{app} the applied tensile pressure, and r_C the elastic-viscoplastic boundary which divides the matrix material into two zones: the inner viscoplastic zone and the outer elastic zone.

$$\eta \equiv \frac{\tau_e}{\dot{\gamma}^p} = \frac{\tau_e}{2f\exp\left(-\frac{\Delta G^m}{k_B T}\right)\sinh\left(\frac{\tau^e \Omega}{2k_B T}\right)\exp\left(-\frac{1}{\xi}\right)} \tag{4}$$

where $\tau_e = \sqrt{J_2} = \sqrt{s_{ij}s_{ij}/2}$ is the effective shear stress, $\dot{\gamma}^p$ is the plastic strain rate, f is the frequency of atomic vibration (∼Debye frequency), ΔG^m is the activation energy, k_B is the Boltzmann constant, Ω is the atomic volume, and ξ is the concentration of free volume ($\xi = v_f/\chi v^*$, here v_f, χ and v^* are, respectively, the free volume, a geometric factor and the effective hard-sphere size of an atom).

The free volume concentration is adopted as an order parameter, which is a function of the radius r in the current configuration and the time t. Following Huang et al. (2002) and Dai et al. (2005), the free volume evolution equation is written as:

$$\frac{\partial \xi}{\partial t} = D\nabla^2 \xi + G(\xi, T, \tau, p) \tag{5}$$

where D is the diffusion coefficient of free volume concentration and $G(\xi, T, \tau, p)$ is the net generation rate of free volume, the explicit expression of which was presented by Spaepen (1977) and is modified here to cover the free volume dependence on pressure

$$G(\xi, T, \tau, p) = \frac{1}{\chi} f \exp\left[-\frac{1}{\xi}\right]\exp\left[-\frac{\Delta G_m}{k_B T}\right]\left\{\frac{2k_B T}{\xi v^* S}\left[\cosh\left(\frac{\tau_e \Omega}{2k_B T}\right) - 1\right] - \frac{1}{n_D}\right\} + \frac{\Omega \dot{p}}{\chi v^* \kappa} \tag{6}$$

where S is the effective shear modulus ($S = \frac{2(1+\nu)\mu}{3(1-\nu)}$ with ν being Poisson's ratio), n_D the number of diffusive jumps necessary to annihilate a free volume equal to v^*, and κ the bulk modulus. Eqs. (5) and (6) indicate that there are three different processes which can change the local free volume concentration, including diffusion, annihilation and generation. In BMGs, the free volume can be redistributed by diffusion until it is spatially uniform. The annihilation of free volume is caused by the atomic rearrangement. Here the generation of free volume is slightly different from the conventional expressions. In addition to the extra free volume created by a shear stress squeezing an atom into a hole smaller than itself, the contribution of volume dilation is considered to take the mean tensile stress effects into account (Flores and Dauskardt, 2001).

As shown in Fig. 1, this is essentially a 1-D problem. So the principle strain can be written as

$$\varepsilon_r = \frac{\partial u_r}{\partial r} \tag{7}$$

$$\varepsilon_\theta = \frac{u_r}{r} \tag{8}$$

where u_r is the displacement. If the matrix material is incompressible, the principle strains satisfy

$$\varepsilon_r + 2\varepsilon_\theta = 0 \tag{9}$$

In fact, the assumption of incompressibility is at odds with the dilation-induced increase of free volume (Steif, 1983). Nevertheless, it does not affect our results. The influence of volume dilation can be divided into two parts: the contribution to the displacement field and the decrease of viscosity. The former could be neglected because the elastic compressibility is so small that the displacement field can be determined from the expansion of the void alone (Carroll and Holt, 1972). But the latter must be taken into account as the viscosity closely depends on the free volume concentration and even very small dilation will induce a remarkable increase of free volume.

In the present framework, the thermal effects are not considered. We think that the role of thermal softening in void growth is similar to that in shear bands (Dai and Bai, 2008; Jiang and Dai, 2009). Although both thermal softening and free volume softening can induce the decrease of viscosity in BMGs, the former is not the primary cause. For the small scale of voids (<1 μm), heat can hardly accumulate in the matrix material. This issue has also been addressed in conventional polycrystalline alloys. As pointed out by Tong and Ravichandran (1995), the effects of thermal softening is relatively small for the dynamic void growth in viscoplastic materials. Wu et al. (2003b) also indicates that the thermal diffusion is strongly affected by the initial void size. The smaller the initial void size is, the more it approaches the athermal case. Their numerical results show that the void growth of 1 μm radius case is similar to the athermal case.

3. Cavitation instabilities

3.1. Analytical results

As BMGs are pressure sensitive materials, the criterion of cavitation instabilities should be different from the traditional ones. To get out this criterion, let us consider the quasistatic case. Then in the spherical coordinates, Eq. (1) can be simplified as the equation of equilibrium, that is

$$\frac{d\sigma_r}{dr} + \frac{2}{r}(\sigma_r - \sigma_\theta) = 0 \tag{10}$$

with the boundary conditions

$$\sigma_r|_{r=a} = 0 \text{ and } \sigma_r|_{r=\infty} = p^{app} \tag{11}$$

If the applied loading is sufficiently high, the void surface yields and the matrix material around the void is divided into two zones: the elastic and viscoplastic zones. In the elastic zone $r \geqslant r_C$, according to the classic elasticity theory, the stress components and radial displacement can be obtained as

$$\sigma_r = p^{app} - \frac{4[\hat{\tau} - (C_1 T/T_g)^{1/2} - Qp^{app}]r_C^3}{3r^3} \tag{12}$$

$$\sigma_\theta = p^{app} + \frac{2[\hat{\tau} - (C_1 T/T_g)^{1/2} - Qp^{app}]r_C^3}{3r^3} \tag{13}$$

$$u_r = \frac{[\hat{\tau} - (C_1 T/T_g)^{1/2} - Qp^{app}]r_C^3}{3\mu r^2} \tag{14}$$

In the viscoplastic zone $a \leqslant r \leqslant r_C$, as BMGs are regarded as viscoplastic materials, the yield criterion must be obeyed when the viscous flow stops. So in this zone, the equilibrium equation becomes

$$\frac{d\sigma_r}{dr} = \frac{-12Q\sigma_r + 12\hat{\tau} - 12(C_1 T/T_g)^{1/2}}{(3+4Q)r} \tag{15}$$

Using the boundary condition at $r = a$ and the continuous condition of radial stress σ_r across the elastic-viscoplastic boundary, we can obtain

$$p^{app} = \frac{\hat{\tau} - (C_1 T/T_g)^{1/2}}{Q} - \frac{3[\hat{\tau} - (C_1 T/T_g)^{1/2}]a^{12Q/(3+4Q)}}{Q(3+4Q)r_C^{12Q/(3+4Q)}} \tag{16}$$

To calculate the void radius a, the equation of incompressibility is used to provide additional information. Similar to Hill's analysis (Hill, 1950), the elastic-viscoplastic boundary r_C is taken as the scale of "time", and the velocity v of a particle means that the particle is displaced by an amount vdr_C when the elastic-viscoplastic boundary moves outwards a further distance dr_C. Thus, we have

$$v = \frac{\partial u_r/\partial r_C}{1 - (\partial u_r/\partial r)} \tag{17}$$

and Eq. (9) is rewritten as

$$\frac{\partial v}{\partial r}+\frac{2v}{r}=0 \tag{18}$$

On the elastic-viscoplastic boundary, v can be calculated from Eqs. (14) and (17), that is

$$v|_{r=r_C}=\frac{\hat{\tau}-(C_1T/T_g)^{1/2}-Qp^{app}}{\mu} \tag{19}$$

Solving Eq. (18) with the boundary condition Eq. (19), leads to

$$v=\frac{[\hat{\tau}-Qp^{app}-(C_1T/T_g)^{1/2}]r_C^2}{\mu r^2} \tag{20}$$

On the inner surface, $v = da/dr_C$, so the relation between a and r_C is

$$\frac{da}{dr_C}=\frac{[\hat{\tau}-Qp^{app}-(C_1T/T_g)^{1/2}]r_C^2}{\mu a^2} \tag{21}$$

Then, combining Eqs. (16) and (21) yields

$$\frac{a^3}{A^3}=\frac{\left[\hat{\tau}-(C_1T/T_g)^{1/2}-Qp^{app}\right]r_C^3}{\mu A^3}+\left[1-\frac{3\hat{\tau}-3(C_1T/T_g)^{1/2}}{\mu(3+4Q)}\right]\Big/\left[1-\frac{\hat{\tau}-(C_1T/T_g)^{1/2}}{\mu(3+4Q)}\right]^3 \tag{22}$$

Once cavitation instabilities occur, the relative void size goes to infinity, i.e., $a/A\to\infty$ or $A\to 0$. Then, in terms of the void size, the position of the elastic-viscoplastic boundary is

$$\frac{r_C}{a}=\left(\frac{\mu}{\hat{\tau}-Qp^{app}-(C_1T/T_g)^{1/2}}\right)^{1/3} \tag{23}$$

Thus, with Eqs. (16) and (23), the critical pressure for cavitation instabilities in BMGs is

$$p_{cr}^{app}=\frac{\hat{\tau}-(C_1T/T_g)^{1/2}}{Q}-\frac{1}{Q\mu^{4Q/3}}\left(\frac{3\hat{\tau}-3(C_1T/T_g)^{1/2}}{3+4Q}\right)^{(3+4Q)/3} \tag{24}$$

Using the material parameters (Sun et al., 2010) $\hat{\tau}-(C_1T/T_g)^{1/2}=823.2\ MPa$ and $\mu = 35.3$ GPa for a typical metallic glass Vit. 1, the critical pressure for cavitation instabilities versus the pressure sensitivity coefficient is shown in Fig. 2. The cavitation pressure decreases as the pressure sensitivity coefficient increases (the actual pressure sensitivity coefficient for Vit. 1 is 0.158).

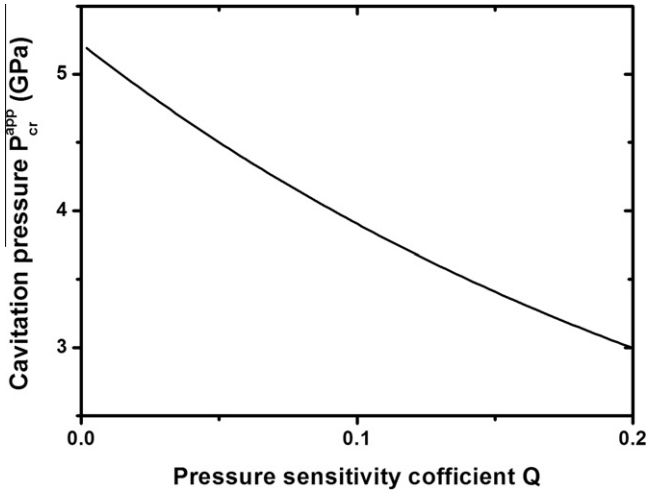

Fig. 2. The cavitation pressure as a function of pressure sensitivity coefficient.

Because the pressure sensitivity stimulates the yield of a material under hydrostatic tensile loading, cavitation instabilities prefer to occur in solids with a higher pressure sensitivity coefficient.

3.2. Numerical results

As a comparison with the theoretical result, the full set of Eqs. (2)–(11) are solved numerically with the finite difference method (FDM). To avoid dealing with an infinite time-dependent domain, a time-dependent coordinate transformation (Bouchbinder et al., 2008) is applied

$$x=\frac{a(t)}{r} \tag{25}$$

Thus, integration of equations in the time-independent finite domain $x\in(0,1)$ is allowed. This transformed space domain is uniformly discretized with 1001 nodes, while the time domain is discretized with 100001 nodes. Each result is checked to make sure that it will not change with increasing the node number.

Fig. 3 shows the history of hydrostatic tensile loading which is applied on the outer boundary ($x = 0$). For comparison with relevant works (Ortiz and Molinari, 1992; Wu et al., 2003b), a similar form of the applied pressure is adopted. As displayed in Fig. 3, the loading history is divided to two stages: the rise stage in which the applied pressure increases linearly until the desired loading amplitude p_S is achieved after a rise time t_a, and the steady stage in which the loading is held constant at p_S during the hold time t_S. A typical metallic glass Vit. 1 is chosen as a model material in this paper, and its mechanical and physical parameters derived from other literatures (Faupel et al., 2003; Jiang and Dai, 2009; Jiang et al., 2008; Lu et al., 2003; Yang et al., 2006) are listed in Table 1. For FDM simulations, the initial void sizes A and the loading amplitudes p_S are chosen based on experiments. As the diameters of observed void/dimple patterns on fracture surfaces always lie between 100 nm to 10 μm (Bouchaud et al., 2008; Escobedo and Gupta, 2010; Huang et al., 2011; Jiang et al., 2008; Meng et al., 2008; Qu et al., 2010; Zhuang et al., 2002), the initial void radius A varies from 10 nm to micrometer length scale. Besides, according to the predicted cavitation pressure (3.34 GPa for Vit. 1 in Section 3.1), the loading amplitude p_S is chosen ranging from 2 GPa to 4 GPa. This range is close to the applied loading amplitude in spallation experiments (Atroshenko et al., 2010; Huang et al., 2011; Turneaure et al., 2007; Yuan et al., 2007).

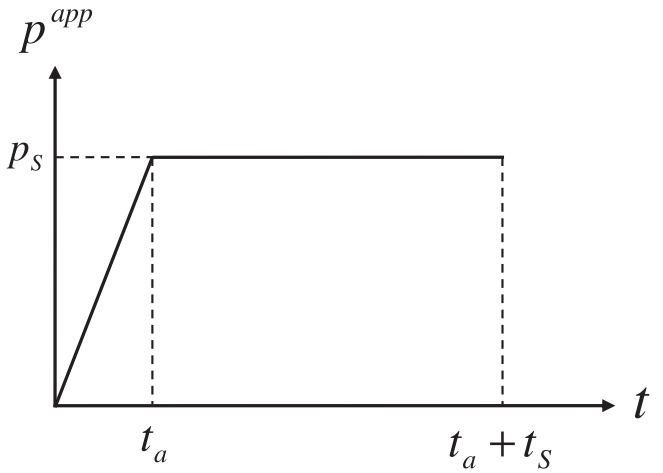

Fig. 3. Loading history of applied tensile pressure. The loading history contains two stages: the rise stage in which the applied pressure increases linearly until the desired loading p_S is achieved after a rise time t_a, and the steady stage in which the loading is held constant at p_S during the hold time t_S.

Table 1
Material parameters for Vit. 1.

Parameters	Notation	Value
Shear modulus	μ	35.3 GPa
Density	ρ	6125 Kg m^{-3}
Free-volume diffusivity	D	$\sim 10^{-16}$ m^2 s^{-1}
Average atomic volume	Ω	20 A^3
Activation energy	ΔG^m	0.2–0.5 eV
Frequency of atomic vibration	f	$\sim 10^{13}$ s^{-1}
Boltzmann constant	k_B	13.8×10^{-24} J/K
Pressure sensitivity coefficient	Q	0.158
Glass transition temperature	T_g	638 K
Geometric factor	χ	0.105
Effective hard-sphere size of atom	v^*	20 A^3
Bulk modulus	K	112.7 GPa
Effective shear modulus	S	50.0 GPa
Jump number for annihilation	n_D	6

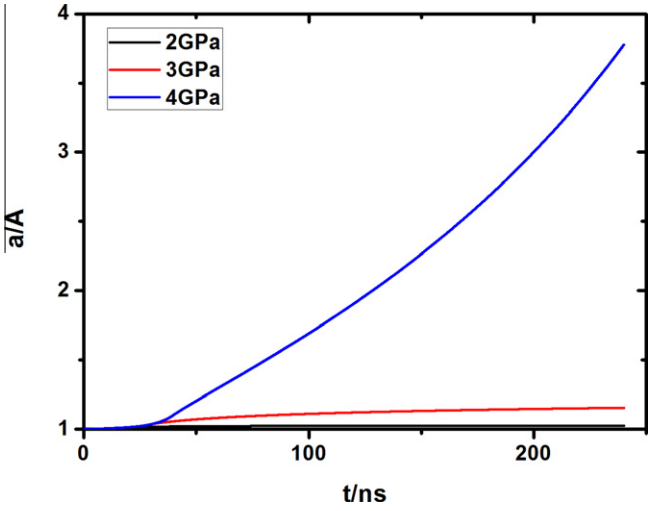

Fig. 4. Numerical results on void growth under different loading amplitudes. The loading increases linearly after a same rise time t_a of 40 ns, and is held at different amplitudes: (a) p_S = 2 GPa; (b) p_S = 3 GPa; (c) p_S = 4 GPa.

In order to estimate the cavitation pressure via the numerical method, the influence of loading amplitudes on the void growth is examined. Consider three cases with the loading amplitude p_S ranging from 2 GPa to 4 GPa, but other parameters remain the same. In each case, the initial void size A is 10 nm, the ambient temperature T_i = 300 K, initial free volume concentration ξ_i = 0.05, and the loading rate q = 0.1 GPa/ns. Fig. 4 shows the numerical results of void growth under different loading amplitudes. Comparing the three cases, a critical pressure p_{cr}^{app} for unbounded growth of voids exists between 3 GPa and 4 GPa. For the amplitudes of 2 GPa and 3 GPa, the growth of voids stops gradually after rapid growth at the early stage. However, as the amplitude increases to 4 GPa, the void never stops growing while the applied loading is held. This numerical result is in consistence with the analytical result in Section 3.1.

4. Dynamic growth of voids

4.1. Scaling of the governing equations

Different from the quasistatic cases, dynamic growth of voids are more complicated. As the equation of equilibrium (Eq. (10)) is replaced by Eq. (1), inertial effects are introduced and other factors such as loading rate effects and viscous effects should be considered carefully. To reveal the dominant factor that controls the void growth, usually one needs to scale the governing equations first.

Among the governing equations, Eq. (1) is the most important, because it contains an acceleration term, i.e. inertial term on the right side which reflects the change of growth rate. To closely estimate the term's order of magnitude, we try to select proper scales to obtain a dimensional factor. For the left side of Eq. (1), it is better to choose the initial void radius A and the loading amplitude p_S as the scales of space and stress. It is worth noting that void growth is a problem with variable boundary, when the void grows significantly larger than the initial one, the current void radius a will become more proper as the scale of space. But for right side of Eq. (1), except for the scale of space A, an unknown scale of time still exists. If t_k is denoted as the time scale, the scaled equation is

$$\frac{d\tilde{\sigma}_r}{d\tilde{r}} + \frac{2(\tilde{\sigma}_r - \tilde{\sigma}_\theta)}{\tilde{r}} = \frac{\rho A^2/p_S}{t_k^2}\ddot{\tilde{r}} \tag{26}$$

where $\tilde{\sigma}_r = \sigma_r/p_S$, $\tilde{r} = r/A$, $\tilde{\sigma}_\theta = \sigma_\theta/p_S$, and $\ddot{\tilde{r}} = \ddot{r}t_k^2/A$. In this way, $\frac{\rho A^2/p_S}{t_k^2}$ is the proper estimation of the order of acceleration term.

Now, the question is in what time scale, a void growth process is well scaled? To answer the question, we should find all the characteristic time scales of physical processes that influence the void growth first. As described in the governing Eqs. (1)–(5), there are three basic processes existed: the outward flux of matter, the deformation of matrix material and the evolution of free volume concentration. In fact, as the viscous flow has already reflected the influence of free volume concentration, only the former two processes need to be considered. For the first process, selecting the proper scales of force, mass and length, the characteristic time scale is determined. Here we think that $\sqrt{\rho A^2/p_S}$ is a proper estimate for the characteristic time scale of outward flux of matter, which has already existed in $\frac{\rho A^2/p_S}{t_k^2}$. For the second process, there is a characteristic time scale of deformation existed. Since the deformation rate of matrix material directly influences void growth rate, this time scale is a proper choice for t_k.

The deformation of matrix material consists of two parts: the elastic part and the viscoplastic part. Thus, as a deformation time scale, t_k should characterize the two parts at the same time. With the constitutive law, we can find an approximation for t_k. For the left side of Eq. (3), choosing $\varepsilon_k = p_S/2\mu$ as the scale of strain, we obtain

$$\dot{\varepsilon}_{ij} \approx \frac{\varepsilon_k}{t_k} = \frac{p_S/(2\mu)}{t_k} \tag{27}$$

Similarly, choosing p_S/t_a as an estimation of $\dot{s}_{ij}$ and p_S as an estimation s_{ij}, the right side of Eq. (3) can be written as

$$\frac{\dot{s}_{ij}}{2\mu} + \frac{s_{ij}}{2\eta} \approx \frac{p_S/t_a}{2\mu} + \frac{p_S}{2\eta} \tag{28}$$

In order to find an uniform expression for t_k, only the viscoplastic part of the constitutive law is used here. Eq. (28) is also applicable for the elastic region. Below the yield point, η can be regarded as infinity, and the term $p_S/(2\eta)$ equals zero. Thus, Eq. (28) is reduced to a form obtained by the elastic part of the constitutive law (Eq. (2)). With Eqs. (3), (27) and (28), we have

$$\frac{1}{t_k} = \frac{1}{t_a} + \frac{1}{\eta/\mu} \tag{29}$$

As t_k is determined, the dimensional factor used to estimate the order of magnitude of the acceleration term can be obtained. Here we define a dimensionless number which is the square root of the dimensional factor, that is

$$I_{inertia} = \frac{\sqrt{\rho A^2/p_S}}{t_a} + \frac{\sqrt{\rho A^2/p_S}}{\eta/\mu} \tag{30}$$

where $I_{inertia}$ is a dimensionless number similar to the Deborah number and consists of three characteristic time scales: (1) the inertial time scale $t_{inertia} = A/\sqrt{p_S/\rho}$, a characteristic time scale of the outward flux of matter; (2) the loading time scale t_a, which is just the rise time of the loading history; and (3) the relaxation time scale $t_r = \eta/\mu$, a characteristic time for viscous flow. The three time scales represent inertial, loading rate and viscous effects respectively.

4.2. Numerical results on dynamic void growth

Note that the inertial time scale $t_{inertia}$ consists of the initial void radius A, the density ρ and the loading amplitude p_S. To control the dimensionless number $I_{inertia}$, it is convenient to change the initial void radius A. We consider four dynamic cases with different initial void radii which are 100 nm, 1 μm, 5 μm, and 10 μm respectively, and a quasistatic case is presented as a comparison. In each case, the loading amplitude is 4 GPa, the loading rate $q = 0.1$ GPa/ns, the ambient temperature $T_i = 300$ K, and the initial free volume concentration $\xi_i = 0.05$. Fig. 5 shows the numerical results on dynamic void growth with different void radii under the loading of 4 GPa, and the detailed results at the rise stage are presented in Fig. 6. According to the numerical results displayed in Figs. 5 and 6 and the interpretation of the dimensionless number $I_{inertia}$, the void growth process in metallic glass can be divided into three stages, each of which shows different characteristics and is controlled by different part of the dimensionless number $I_{inertia}$.

As shown in Fig. 6, the first stage is the initial part of the rise stage when most of the matrix material deforms below the yield point. In this stage, a transition from smooth growth to vibrating growth occurs as A increases from 100 nm to 10 μm. The larger the value of A is, the higher vibration frequency and the larger vibration amplitude is obtained. Then what is the reason for such a vibrating growth phenomenon?

To understand this, we should examine the dimensionless number $I_{inertia}$ during the first stage. As the applied loading is not very high in this stage, most of the matrix material surrounding the void deforms elastically. At this time, the relaxation time scale $t_r = \infty$ since the viscosity η can be regarded as infinite. Thus the second term of $I_{inertia}$ is equal to zero, and $I_{inertia}$ is simplified to I_1 as follows

$$I_{inertia} = I_1 = \frac{t_{inertia}}{t_a} \tag{31}$$

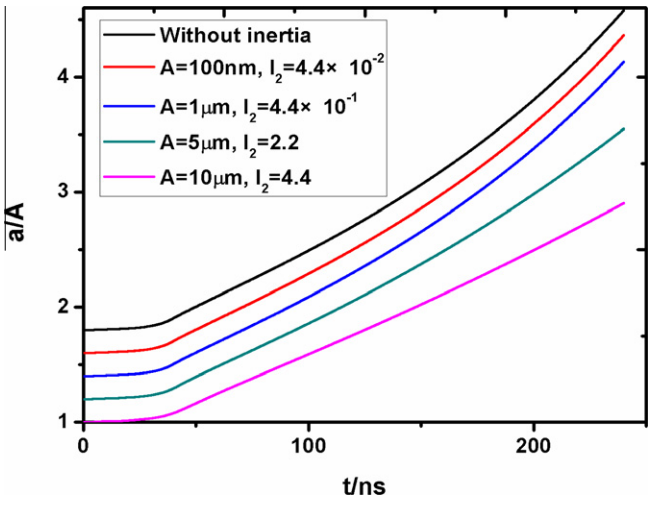

Fig. 5. Dynamic void growth with different initial void radii under the same loading. The rise time t_a is 40 ns, and the loading amplitude p_s is 4 GPa. Five cases are considered: (a) A quasistatic case without inertial effects; (b) $A = 100$ nm, corresponding to the dimensionless number $I_2 = 4.4 \times 10^{-2}$; (c) $A = 1$ μm, $I_2 = 4.4 \times 10^{-1}$; (d) $A = 5$ μm, $I_2 = 2.2$; (e) $A = 10$ μm, $I_2 = 4.4$.

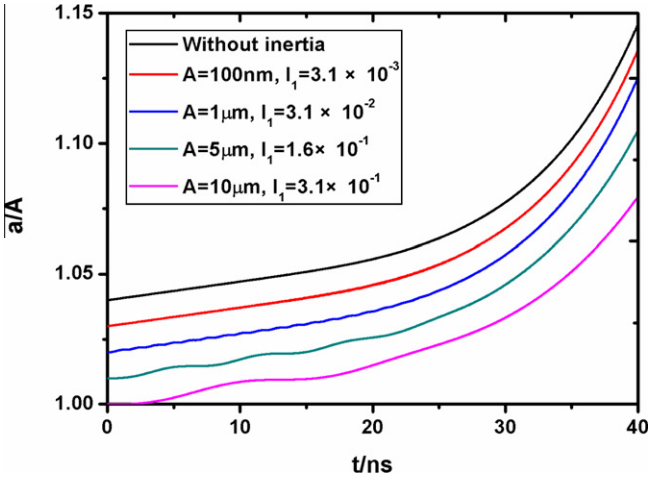

Fig. 6. Detailed results of dynamic void growth at the rise stage. The rise time t_a is 40 ns, and the loading amplitude p_s is 4 GPa. Five cases are considered: (a) A quasistatic case without inertial effects; (b) $A = 100$ nm, corresponding to the dimensionless number $I_1 = 3.1 \times 10^{-3}$; (c) $A = 1$ μm, $I_1 = 3.1 \times 10^{-2}$; (d) $A = 5$ μm, $I_1 = 1.6 \times 10^{-1}$; (e) $A = 10$ μm, $I_1 = 3.1 \times 10^{-1}$.

where I_1 is controlled by the internal microscopic time scale $t_{inertia}$ and the external macroscopic time scale t_a. Since t_a is a constant during the whole rise stage, the variation of I_1 is determined by $t_{inertia}$ alone. As is defined above, $t_{inertia} = A/\sqrt{p_S/\rho}$, which is determined by the initial void radius when the loading amplitude keeps constant. While A increases from 100 nm to 10 μm, I_1 changes from 10^{-3} to 10^{-1}, implying a higher order of the acceleration term. In fact, during the dynamic void growth process, the current void radius usually deviates from a value that the system is in static equilibrium, and the acceleration term can be regarded as a measure of the deviation. Then the larger I_1 is, the higher vibration amplitude of void radius appears.

The change of I_1 cannot explain the change in vibration frequency. This vibration in void growth is actually the elastic oscillation of the void inner surface, similar to a spring-mass system. With the theory of elastic mechanics, the characteristic period for oscillation can be determined to be

$$T = \pi\sqrt{\frac{\rho a^2}{\mu}} \tag{32}$$

where T is the oscillation period, ρ the density of matrix material, a the current void radius, μ the shear modulus. Eq. (32) shows that the oscillation period is controlled by the current void radius alone, because other parameters are the material properties. Therefore the change of vibration frequency is due to the difference of void radii. As illustrated in Fig. 6, the vibration frequency consists with the results predicted by Eq. (32).

Meanwhile, in Fig. 6, $I_1 = 10^{-2}$ seems to be a transition boundary. When $I_1 > 10^{-2}$, strong vibration indicates that the inertial effects, impeding and promoting the growth rate alternatively, dominate the void growth process. But when $I_1 < 10^{-2}$, the void can grow smoothly with the increase of applied loading and the growth rate is controlled by the loading rate effects.

To further study the vibration phenomenon, the influence of the rise time t_a on dynamic void growth is examined. We consider 3 cases with different values of t_a which are 2 ns, 20 ns, and 200 ns respectively, but other parameters remain the same. For each case, the loading amplitude is 2 GPa, the initial void radius 1 μm, the ambient temperature $T_i = 300$ K, and the initial free volume concentration $\xi_i = 0.05$. Fig. 7 shows the void growth with different rise time under the loading of 2 GPa. While I_1 gets larger or the inertial

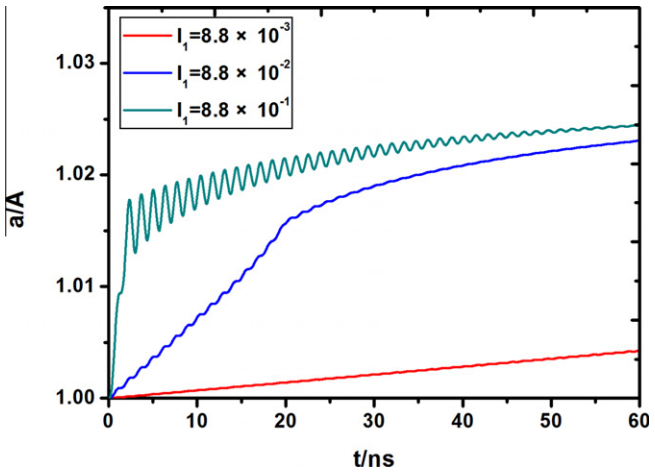

Fig. 7. Void growth with different rise time under the same loading amplitude of 2 GPa. The initial void radius is 1 μm. Three cases are considered: (a) $t_a = 2$ ns, corresponding to the dimensionless number $I_1 = 8.8 \times 10^{-1}$; (b) $t_a = 20$ ns, $I_1 = 8.8 \times 10^{-2}$; (c) $t_a = 200$ ns, $I_1 = 8.8 \times 10^{-3}$.

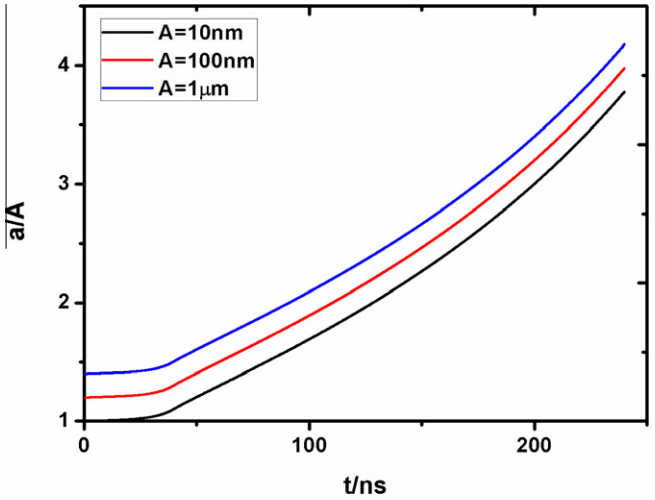

Fig. 8. Quasistatic void growth with different initial void radii under the same loading. The rise time t_a is 40 ns, and the loading amplitude p_s is 4 GPa. Three cases are considered: (a) $A = 10$ nm; (b) $A = 100$ nm; (c) $A = 1$ μm.

effects are more dominant, the vibration amplitude of void growth becomes higher. The transition boundary still lies at $I_1 = 10^{-2}$. For the cases of $I_1 > 10^{-2}$, the inertial effects dominate the void growth and the vibrating growth of void is obvious. For the cases of $I_1 < 10^{-2}$, however, the vibration almost disappears. Moreover, as the initial void radius keeps a constant, the vibration frequency does not change, which is different from the cases shown in Fig. 6. Another difference is the lower loading amplitude, resulting in suppression of the viscous flow of matrix material. And then the vibration disappears gradually, until the oscillation energy is completely dissipated.

The second stage is the latter part of the rise stage. While the applied loading is higher than the yield strength, void growth becomes more complicated duo to the viscous effects. As shown in Fig. 6, the vibration of void growth disappears promptly while the growth rate increases a lot. Actually, with the increase of the applied loading, viscous flow becomes easier as t_r decreases fast from ∞ to the magnitude of 10^{-9} s. Since t_r is shorter than t_a which is the magnitude of 10^{-8} s, the second term of $I_{inertia}$ gets larger than the first term. Thus, $I_{inertia}$ cannot be simplified to I_1 any longer. The void growth is controlled by all the inertial, loading rate and viscous effects. The viscous effects introduce extra energy dissipation for the oscillation of the void's inner surface, therefore cause the oscillation to decay in amplitude towards zero. Besides, the viscous flow significantly increases the deformation rate of matrix material, and then induces the void to grow faster. In fact, the second stage can be regarded as a transition period when the loading rate effects are gradually replaced by the viscous effects.

The third stage is the steady stage of the loading history. As the applied loading stops increasing, the loading rate effects do not exist. Thus, $I_{inertia}$ is simplified to I_2 as

$$I_{inertia} = I_2 = \frac{t_{inertia}}{t_r} \tag{33}$$

Eq. (33) shows that, in the steady stage, the void growth is controlled by the competition of inertial and viscous effects. To calculate I_2, the viscous coefficient influenced by the free volume concentration, should be determined first. As the free volume concentration does not change a lot at this stage (details will be shown in the following Section 4.3), the viscous coefficient nearly keeps constant. Using $\eta \approx 100$ Pa·s, on the inner surface of the void, I_2 can be obtained. As shown in Fig. 5, as I_2 increases from 10^{-2} to 10^{1}, the growth rate decreases gradually. There is a boundary at $I_2 = 1$ among all the cases. If $I_2 < 1$, the results are similar to the case without inertia, implying that the viscous effects are more dominant than the inertial effects. But as I_2 keeps increasing across the boundary, the growth rate slows down. The void growth is significantly impeded as the inertial effects prevail.

According to Eq. (33), the boundary $I_2 = 1$ determines a critical void size, that is

$$A_{cr} = \frac{\eta\sqrt{p_S/\rho}}{\mu} \tag{34}$$

Once the radius is larger than the critical value, the inertial effects significantly reduce the void size. For Vit. 1 under the loading amplitude of 4 GPa, A_{cr} is 2.3 μm. In quasistatic tests, the reported dimple diameter is usually less than 10 μm (Bouchaud et al., 2008; Jiang et al., 2008; Qu et al., 2010). While in dynamic tensile experiments, finer dimples or voids with diameters from 10^2 nm to 5 μm were observed (Escobedo and Gupta, 2010; Huang et al., 2011; Meng et al., 2008; Zhuang et al., 2002). It is likely that the inertial effects impede the generation of larger voids during the fracture process. The above results also prove that the inertial effects prefer to work at the late stage of a void-dominated fracture process.

4.3. Free volume dynamics

For the early stage of a void-dominated fracture process in BMGs, the void radius is usually less than 1 μm. This means that the inertial effects can be neglected, and the viscous effects play a dominant role. In BMGs, microscopic flow events are related to free volume, which is thought to be their intrinsic defects (Spaepen, 1977). Thus the ability of the materials to undergo viscous flow depends closely upon the free volume concentration.

As indicated by Wu et al. (2003b), thermally diffusive cases are strongly affected by the initial void size, because of the length scale introduced by the thermal diffusion. Similar to the thermal diffusion, free volume diffusion will introduce a length scale as well. To address the influence on void growth, we consider four cases with the initial void radius ranging from 10 nm to 1 μm, but other parameters remain the same. For each case, the loading amplitude p_S is 4 GPa, the loading rate $q = 0.1$ GPa/ns, the ambient temperature $T_i = 300$ K, and the initial free volume concentration $\xi_i = 0.05$. Fig. 8 shows the numerical results of quasistatic void growth with different void radii. Different from thermal diffusion cases presented by Wu et al. (2003b), each case is almost the same, therefore

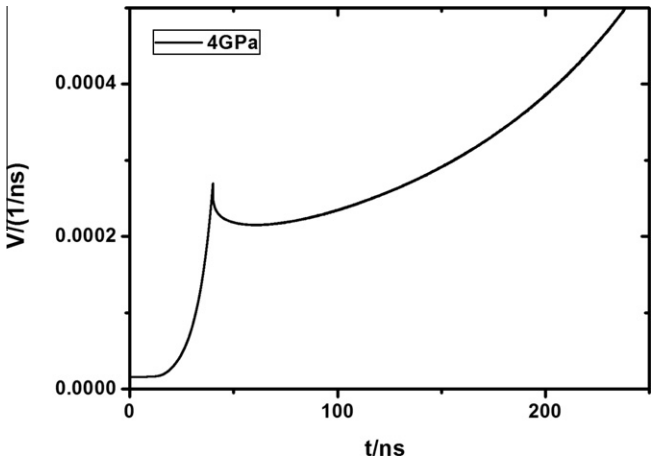

Fig. 9. The history of void growth rate. The rise time t_a is 40 ns, and the loading amplitude p_s is 4 GPa.

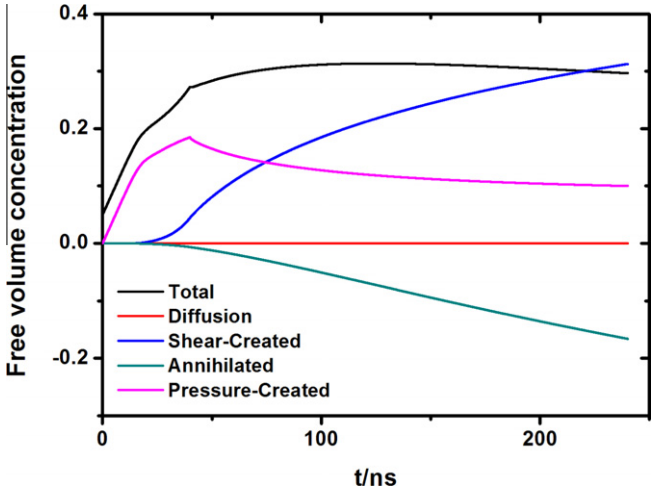

Fig. 10. The evolution of free volume concentration on the inner surface of the void. The rise time t_a is 40 ns, and the loading amplitude p_s is 4 GPa. The terms plotted are: (a) the total free volume concentration; (b) the diffusion term; (c) the shear-created term; (d) the annihilated term; (e) the pressure created term.

the initial void radius has no influence on void growth. As the free volume diffusion coefficient is lower than thermal diffusion coefficient by about ten orders of magnitude, the contribution of free volume diffusion can be neglected.

Fig. 9 presents the history of growth rate ($V = \dot{a}/A$) in the case with the initial void radius of 10 nm. The growth rate changes continuously during the whole loading history. At the rise stage, it holds constant at first and then increases promptly. For the elastic response of matrix material and the linearly increase of applied loading, the growth rate should keep constant. But when the matrix material begins to yield, viscous flow induces a sharp increase of growth rate. At the steady stage, it decreases rapidly first and then increases gradually. As the growth rate is determined by the viscous flow of the matrix material, the evolution of free volume concentration should be further examined.

Fig. 10 shows the evolution of free volume concentration on the inner surface of the void with the initial void radius of 10 nm. As illustrated in Fig. 10, the diffusion term has little contribution to the total free volume during the whole process for the extremely low diffusion coefficient. At the beginning of the rise stage, the increase of total free volume concentration is mainly attributed to the volume dilation induced by hydrostatic tensile pressure. While the applied loading continuously increases, stress relaxation induced by viscous flow will slow down the increase rate of the pressure created term. At the same time, however, the increase of the shear-created term speeds up for the increasing shear stress. When it enters the steady stage, due to the stress relaxation, the pressure created term decreases and the increase of the shear-created term slows down. The annihilated term which is not influenced by the stress state increases at nearly the same rate. But in general, the total free volume concentration does not change a lot at the steady stage.

As the evolution of free volume concentration is addressed, the change in growth rate at the steady stage in Fig. 9 can be understood. At the beginning of this stage, the growth rate drops abruptly since the applied loading stops increasing (The increase of elastic deformation stops). Then it drops gradually. For the free volume concentration does not change a lot, this is caused by the rapid decrease of stresses at the beginning of stress relaxation. In the later part of the steady stage, both the viscosity and stresses are relatively steady. The acceleration of growth rate is due to the significant increase of void radius.

5. Conclusion

This paper presents a theoretical description of void growth undergoing remote hydrostatic tension to understand the void-dominated fracture process in BMGs. Based on theoretical analysis of the material elastic-viscoplastic response, an explicit expression of the critical pressure for cavitation instabilities is obtained. It is shown that cavitation instabilities prefer to occur in solids with higher pressure sensitivity coefficient. The theoretical results are validated numerically by FDM simulations on quasistatic growth of voids in BMGs.

For the dynamic void growth, a dimensionless number is proposed to characterize the dominant factors. This dimensionless number consists of three different time scales which are the inertial time scale, the loading time scale and the relaxation time scale. It reflects the competition of the inertial effects, the loading rate effects and the viscous effects. Via FDM simulations, we found that at the rise stage of the loading history, the competition between the inertial effects and the loading rate effects controls the growth process. A transition boundary of $I_1 = 10^{-2}$ is observed, above which the inertial effects are more dominant and the vibration of growth occurs. While the viscous effects begin to work, the loading rate effects are gradually replaced, and the viscous effects will induce higher growth rate and disappearance of vibrating growth. At the steady stage, the competition between the inertial effects and the viscous effects controls the growth process. A transition boundary lies at $I_2 = 1$. Above the boundary, the inertial effects become dominant and the growth of void is obviously impeded. While below the boundary, void growth is controlled by viscous effects. For the void growth at the early stage of a void-dominated fracture process (void radius less than 1 μm), it is found that void growth rate is strongly influenced by viscous flow of the material which depends on the free volume concentration. And the evolution of free volume is mainly controlled by three processes which are pressure induced generation, shear stress induced generation, and annihilation, while the diffusion of free volume can be neglected during the growth process.

Acknowledgements

Financial support was from the National Key Basic Research Program of China (2012CB937500), the NSFC (Grants Nos.: 11272328, 11132011, 11021262, 11002144 and 10872206), and the National Natural Science Foundation of China-NSAF. Grant No: 10976100.

Appendix A. Supplementary data

Supplementary data associated with this article can be found, in the online version, at http://dx.doi.org/10.1016/j.ijsolstr.2013.01.011.

References

An, Q., Garrett, G., Samwer, K., Liu, Y., Zybin, S.V., Luo, S.-N., Demetriou, M.D., Johnson, W.L., Goddard, W.A., 2011. Atomistic characterization of stochastic cavitation of a binary metallic liquid under negative pressure. J. Phys. Chem. Lett. 2, 1320–1323.

Argon, A.S., 1979. Plastic-deformation in metallic glasses. Acta Metall. 27, 47–58.

Arman, B., Luo, S.-N., Germann, T.C., Çağın, T., 2010. Dynamic response of $Cu_{46}Zr_{54}$ metallic glass to high-strain-rate shock loading: plasticity, spall, and atomic-level structures. Phys. Rev. B 81, 144201.

Atroshenko, S.A., Morozov, N.F., Zheng, W., Huang, Y.J., Sudenkov, Y.V., Naumova, N.S., Shen, J., 2010. Deformation behaviors of a TiZrNiCuBe bulk metallic glass under shock loading. J. Alloys Compd. 505, 501–504.

Ball, J.M., 1982. Discontinuous equilibrium solutions and cavitation in nonlinear elasticity. Philos. Trans. R. Soc. London, A 306, 557–611.

Bouchaud, E., Boivin, D., Pouchou, J.L., Bonamy, D., Poon, B., Ravichandran, G., 2008. Fracture through cavitation in a metallic glass. EPL Europhys. Lett. 83, 66006.

Bouchbinder, E., Langer, J.S., Procaccia, I., 2007a. Athermal shear-transformation-zone theory of amorphous plastic deformation. I. Basic principles. Phys. Rev. E 75, 036107.

Bouchbinder, E., Langer, J.S., Procaccia, I., 2007b. Athermal shear-transformation-zone theory of amorphous plastic deformation. II. Analysis of simulated amorphous silicon. Phys. Rev. E 75, 036108.

Bouchbinder, E., Lo, T.S., Procaccia, I., 2008. Dynamic failure in amorphous solids via a cavitation instability. Phys. Rev. E 77, 025101.

Carroll, M.M., Holt, A.C., 1972. Static and dynamic pore-collapse relations for ductile porous materials. J. Appl. Phys. 43, 1626–1636.

Chen, M.W., 2008. Mechanical behavior of metallic glasses: microscopic understanding of strength and ductility. Annu. Rev. Mater. Res. 38, 445–469.

Chen, Y., Jiang, M.Q., Wei, Y.J., Dai, L.H., 2011. Failure criterion for metallic glasses. Philos. Mag. 91, 4536–4554.

Dai, L.H., Bai, Y.L., 2008. Basic mechanical behaviors and mechanics of shear banding in BMGs. Int. J. Impact Eng. 35, 704–716.

Dai, L.H., Yan, M., Liu, L.F., Bai, Y.L., 2005. Adiabatic shear banding instability in bulk metallic glasses. Appl. Phys. Lett. 87, 141916.

Egami, T., 2011. Atomic level stresses. Prog. Mater. Sci. 56, 637–653.

Escobedo, J.P., Gupta, Y.M., 2010. Dynamic tensile response of Zr-based bulk amorphous alloys: fracture morphologies and mechanisms. J. Appl. Phys. 107, 123502.

Falk, M.L., Langer, J.S., 1998. Dynamics of viscoplastic deformation in amorphous solids. Phys. Rev. E 57, 7192–7205.

Falk, M.L., Langer, J.S., 2011. Deformation and failure of amorphous, solidlike materials. Annu. Rev. Condens. Matter Phys. 2, 353–373.

Faupel, F., Frank, W., Macht, M.P., Mehrer, H., Naundorf, V., Ratzke, K., Schober, H.R., Sharma, S.K., Teichler, H., 2003. Diffusion in metallic glasses and supercooled melts. Rev. Mod. Phys. 75, 237–280.

Flores, K.M., Dauskardt, R.H., 2001. Mean stress effects on flow localization and failure in a bulk metallic glass. Acta Mater. 49, 2527–2537.

Gao, Y.F., Yang, B., Nieh, T.G., 2007. Thermomechanical instability analysis of inhomogeneous deformation in amorphous alloys. Acta Mater. 55, 2319–2327.

Gao, Y.F., Wang, L., Bei, H., Nieh, T.G., 2011. On the shear-band direction in metallic glasses. Acta Mater. 59, 4159–4167.

Greer, A.L., 1995. Metallic glasses. Science 267, 1947–1953.

Greer, J.R., De Hosson, J.T.M., 2011. Plasticity in small-sized metallic systems: intrinsic versus extrinsic size effect. Prog. Mater. Sci. 56, 654–724.

Greer, A.L., Ma, E., 2007. Bulk metallic glasses: at the cutting edge of metals research. MRS Bull. 32, 611–615.

Han, Z., Wu, W.F., Li, Y., Wei, Y.J., Gao, H.J., 2009. An instability index of shear band for plasticity in metallic glasses. Acta Mater. 57, 1367–1372.

Hill, R., 1950. The Mathematical Theory of Plasticity. Oxford University Press, Oxford.

Horgan, C.O., Abeyaratne, R., 1986. A bifurcation problem for a compressible nonlinearly elastic medium: growth of a micro-void. J. Elast. 16, 189–200.

Huang, Y., Hutchinson, J.W., Tvergaard, V., 1991. Cavitation instabilities in elastic–plastic solids. J. Mech. Phys. Solids 39, 223–241.

Huang, R., Suo, Z., Prevost, J.H., Nix, W.D., 2002. Inhomogeneous deformation in metallic glasses. J. Mech. Phys. Solids 50, 1011–1027.

Huang, X., Ling, Z., Zhang, H.S., Ma, J., Dai, L.H., 2011. How does spallation microdamage nucleate in bulk amorphous alloys under shock loading? J. Appl. Phys. 110, 103519.

Jiang, M.Q., Dai, L.H., 2009. On the origin of shear banding instability in metallic glasses. J. Mech. Phys. Solids 57, 1267–1292.

Jiang, M.Q., Dai, L.H., 2011. Shear-band toughness of bulk metallic glasses. Acta Mater. 59, 4525–4537.

Jiang, M.Q., Ling, Z., Meng, J.X., Dai, L.H., 2008. Energy dissipation in fracture of bulk metallic glasses via inherent competition between local softening and quasi-cleavage. Philos. Mag. 88, 407–426.

Jiang, M.Q., Ling, Z., Meng, J.X., Gao, J.B., Dai, L.H., 2010a. Nanoscale periodic corrugation to dimple transition due to "beat" in a bulk metallic glass. Scripta Mater. 62, 572–575.

Jiang, M.Q., Meng, J.X., Gao, J.B., Wang, X.L., Rouxel, T., Keryvin, V., Ling, Z., Dai, L.H., 2010b. Fractal in fracture of bulk metallic glass. Intermetallics 18, 2468–2471.

Johnson, J.N., 1981. Dynamic fracture and spallation in ductile solids. J. Appl. Phys. 52, 2812–2825.

Johnson, W.L., 1999. Bulk glass-forming metallic alloys: science and technology. MRS Bull. 24, 42–56.

Joshi, S., Ramesh, K., 2008. Stability map for nanocrystalline and amorphous materials. Phys. Rev. Lett. 101, 025501.

Liu, L.F., Dai, L.H., Bai, Y.L., Wei, B.C., 2005. Initiation and propagation of shear bands in Zr-based bulk metallic glass under quasi-static and dynamic shear loadings. J. Non-Cryst. Solids 351, 3259–3270.

Lu, J., Ravichandran, G., Johnson, W.L., 2003. Deformation behavior of the $Zr_{41.2}Ti_{13.8}Cu_{12.5}Ni_{10}Be_{22.5}$ bulk metallic glass over a wide range of strain-rates and temperatures. Acta Mater. 51, 3429–3443.

Martin, M., Thadhani, N.N., Kecskesb, L., Dowding, R., 2006. Instrumented anvil-on-rod impact testing of a bulk metallic glass composite for constitutive model validation. Scripta Mater. 55, 1019–1022.

Martin, M., Kecskesb, L., Thadhani, N.N., 2008. Dynamic compression of a zirconium-based bulk metallic glass confined by a stainless steel sleeve. Scripta Mater. 59, 688–691.

Meng, J.X., Ling, Z., Jiang, M.Q., Zhang, H.S., Dai, L.H., 2008. Dynamic fracture instability of tough bulk metallic glass. Appl. Phys. Lett. 92, 171909.

Molinari, A., Mercier, S., 2001. Micromechanical modelling of porous materials under dynamic loading. J. Mech. Phys. Solids 49, 1497–1516.

Murali, P., Guo, T., Zhang, Y., Narasimhan, R., Li, Y., Gao, H., 2011. Atomic scale fluctuations govern brittle fracture and cavitation behavior in metallic glasses. Phys. Rev. Lett. 107, 215501.

Ortiz, M., Molinari, A., 1992. Effect of strain-hardening and rate sensitivity on the dynamic growth of a void in a plastic material. J. Appl. Mech. Trans. ASME 59, 48–53.

Pan, D., Inoue, A., Sakurai, T., Chen, M.W., 2008. Experimental characterization of shear transformation zones for plastic flow of bulk metallic glasses. Proc. Natl. Acad. Sci. USA 105, 14769–14772.

Qu, R.T., Stoica, M., Eckert, J., Zhang, Z.F., 2010. Tensile fracture morphologies of bulk metallic glass. J. Appl. Phys. 108, 063509.

Ruan, H.H., Zhang, L.C., Lu, J., 2011. A new constitutive model for shear banding instability in metallic glass. Int. J. Solids Struct. 48, 3112–3127.

Schuh, C.A., Hufnagel, T.C., Ramamurty, U., 2007. Mechanical behavior of amorphous alloys. Acta Mater. 55, 4067–4109.

Spaepen, F., 1977. A microscopic mechanism for steady state inhomogeneous flow in metallic glasses. Acta Metall. 25, 407–415.

Spaepen, F., 2006. Homogeneous flow of metallic glasses: a free volume perspective. Scripta Mater. 54, 363–367.

Steif, P.S., 1983. Ductile versus brittle behavior of amorphous metals. J. Mech. Phys. Solids 31, 359–388.

Sun, L., Jiang, M.Q., Dai, L.H., 2010. Intrinsic correlation between dilatation and pressure sensitivity of plastic flow in metallic glasses. Scripta Mater. 63, 945–948.

Tong, W., Ravichandran, G., 1995. Inertial effects on void growth in porous viscoplastic materials. J. Appl. Mech. Trans. ASME 62, 633–639.

Trexler, M.M., Thadhani, N.N., 2010. Mechanical properties of bulk metallic glasses. Prog. Mater. Sci. 55, 759–839.

Turneaure, S.J., Dwivedi, S.K., Gupta, Y.M., 2007. Shock-wave induced tension and spall in a zirconium-based bulk amorphous alloy. J. Appl. Phys. 101, 043514.

Tvergaard, V., 2012. On cavitation instabilities with interacting voids. Eur. J. Mech. A. Solid 32, 52–58.

Tvergaard, V., Hutchinson, J.W., 1993. Effect of Initial void shape on the occurrence of cavitation instabilities in elastic–plastic solids. J. Appl. Mech. 60, 807–812.

Tvergaard, V., Vadillo, G., 2007. Influence of porosity on cavitation instability predictions for elastic–plastic solids. Int. J. Mech. Sci. 49, 210–216.

Tvergaard, V., Huang, Y., Hutchinson, J.W., 1992. Cavitation instabilities in a power hardening elastic–plastic solid. Eur. J. Mech. A. Solid 11, 215–231.

Wang, W.H., 2012. The elastic properties, elastic models and elastic perspectives of metallic glasses. Prog. Mater. Sci. 57, 487–656.

Wright, W.J., Hufnagel, T.C., Nix, W.D., 2003. Free volume coalescence and void formation in shear bands in metallic glass. J. Appl. Phys. 93, 1432.

Wu, X.Y., Ramesh, K.T., Wright, T.W., 2003a. The coupled effects of plastic strain gradient and thermal softening on the dynamic growth of voids. Int. J. Solids Struct. 40, 6633–6651.

Wu, X.Y., Ramesh, K.T., Wright, T.W., 2003b. The dynamic growth of a single void in a viscoplastic material under transient hydrostatic loading. J. Mech. Phys. Solids 51, 1–26.

Wu, X.Y., Ramesh, K.T., Wright, T.W., 2003c. The effects of thermal softening and heat conduction on the dynamic growth of voids. Int. J. Solids Struct. 40, 4461–4478.

Yang, Q., Mota, A., Ortiz, M., 2006. A finite-deformation constitutive model of bulk metallic glass plasticity. Comput. Mech. 37, 194–204.

Yuan, F.P., Prakash, V., Lewandowski, J.J., 2007. Spall strength and Hugoniot elastic limit of a zirconium-based bulk metallic glass under planar shock compression. J. Mater. Res. 22, 402–411.

Zhuang, S.M., Lu, J., Ravichandran, G., 2002. Shock wave response of a zirconium-based bulk metallic glass and its composite. Appl. Phys. Lett. 80, 4522–4524.